



UKAEA-CCFE-PR(25)370

Priti Kanth Ivan Kodeli Mark Gilbert

# Uncertainty in C-14 production from oxygen isotopes

Enquiries about copyright and reproduction should in the first instance be addressed to the UKAEA Publications Officer, Culham Science Centre, Building K1/0/83 Abingdon, Oxfordshire, OX14 3DB, UK. The United Kingdom Atomic Energy Authority is the copyright holder.
The contents of this document and all other UKAEA Preprints, Reports and Conference Papers are available to view online free at scientific-publications.ukaea.uk/

## Uncertainty in C-14 production from oxygen isotopes

Priti Kanth Ivan Kodeli Mark Gilbert

#### Uncertainty in <sup>14</sup>C production from oxygen isotopes

Priti Kantha, Ivan Kodelia, Mark Gilberta

<sup>a</sup>UKAEA Culham Science Centre Abingdon UK

#### **Abstract**

<sup>14</sup>C is produced from the activation of N and O with high-energy neutrons. Due to its long half-life, high residence time in the environment and ease of assimilation into living matter, it is a major concern for the transportation of activated material and disposal of radioactive waste materials. This paper reports the discrepancy in the <sup>14</sup>C production from O isotopes, using different data libraries and how that discrepancy would affect radioactive waste assessment and disposal and recycling recommendations. The paper also reports the inconsistencies in the uncertainty data and co-variance matrices given in the nuclear data library.

Keywords: 14C, Radioactive waste, Nuclear data, FISPACT-II

#### 1. Introduction

<sup>14</sup>C is a naturally occurring radioactive isotope produced continuously in the atmosphere by cosmic ray neutrons interacting with atmospheric nitrogen. In fusion reactors, <sup>14</sup>C is produced by the interaction of high-energy fusion neutrons with N and O isotopes. The various production paths for <sup>14</sup>C in fusion materials according to ENDF/B-VIII.0 data library, when irradiated with the DEMO breeder blanket neutron spectrum, are given in Fig. 1. The DEMO spectra were obtained for a 2017 European DEMO baseline design (1; 2). The blue arrows in the graph show direct reactions from a parent to a daughter. The red double-headed arrow corresponds to a loop; <sup>14</sup>N undergoes (n,p) reaction to produce <sup>14</sup>C and <sup>14</sup>C decays to <sup>14</sup>N. The reaction's name and the probability of the creation of the daughter from the parent are written on the edges of the graph. More details on how to create these plots can be found in the paper (3).

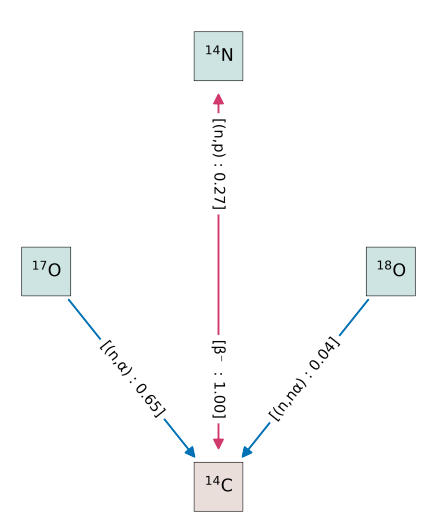


Figure 1: Pathways for production of <sup>14</sup>C using ENDF/B-VIII.0 data library

The production of <sup>14</sup>C from <sup>14</sup>N is well-validated experimentally, and there is good agreement between different nuclear data libraries, see Fig. 2. The same is not true for the case of <sup>14</sup>C production from the isotopes of O. In naturally occurring O, <sup>16</sup>O is most abundant with 99.8% natural abundance, followed by <sup>18</sup>O with 0.205% natural abundance and <sup>17</sup>O with 0.0380%.  $^{17}\mathrm{O}(\mathrm{n},\alpha)^{14}\mathrm{C}$  and  $^{18}\mathrm{O}(\mathrm{n},\mathrm{n}'\alpha)^{14}\mathrm{C}$  reaction cross-section data vary widely between the different nuclear data libraries, and only very few experimental data points are available at high energies. This could lead to high variation in the assessment of <sup>14</sup>C production in the case of water or oxygen-rich materials like mixed oxide fuel (MOX) and KALOS. KALOS is a candidate for the breeder material for EU-DEMO reactors. It is a mixture of LiSiO<sub>4</sub> and LiTiO<sub>3</sub> (4; 5). <sup>14</sup>C is a weak beta emitter and, at normal concentrations, is not a concern for external radiation hazards. However, controlling its release from nuclear facilities becomes important because of its high isotopic exchange rates in living organisms. Details about the regulatory requirements of <sup>14</sup>C are given in (6). Thus, the amount of <sup>14</sup>C generated from KALOS could determine its End-of-life (EOL) processes (7). If the disposal route is opted for, the amount of <sup>14</sup>C would be crucial since various national waste repositories have limits on the amount of <sup>14</sup>C that can be accepted (7; 8). On the other hand, since Lithium is a valuable material in fusion reactors, it would be desirable to recycle KALOS (9). In a recycling process, as <sup>14</sup>C can form various carbon compounds and gases like CO<sub>2</sub> and CO, an accurate assessment of <sup>14</sup>C would be warranted. Thus, to clearly define the EOL recommendation for materials like KALOS, an accurate assessment of 14C is crucial. This paper highlights the difference in <sup>14</sup>C assessment when using different nuclear data libraries and discusses how these differences could affect waste classification and recycling perspective. The paper also reports the inconsistencies in the uncertainty data and co-variance matrices given in the different nuclear data libraries using SUSD3D code (10).

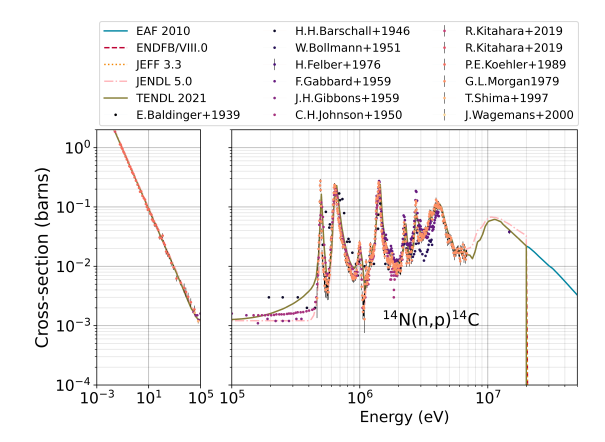


Figure 2: (n,p) Reaction cross-section for <sup>14</sup>C production from <sup>14</sup>N, comparing the evaluations from several different nuclear data libraries with the available experimental data points in EXFOR. The number next to each EXFOR point indicates the year in which the data was published.

#### 2. Nuclear data

To demonstrate the impact of the choice of the nuclear data library on the production of <sup>14</sup>C, the reaction cross-sections from the most commonly used nuclear data libraries are investigated. We consider TENDL 2021 (TALYS-Evaluated Nuclear Data Library developed at IAEA and PSI, Switzerland) (11; 12), JEFF 3.3 (Joint Evaluated Fission and Fusion File produced via an international collaboration of NEA Data Bank participating countries) (13; 14), the 2010 version of the European Activation File (EAF) developed at UKAEA (15), JENDL-5.0 (fifth version of Japanese Evaluated Nuclear Data Library) (16) and ENDF/B-VIII.0 (library from Brookhaven National Lab in the US) (17; 18).

The reaction cross-section for the production of <sup>14</sup>C by <sup>17</sup>O and <sup>18</sup>O for the different nuclear data libraries are given in Figures 3 and 4. The figures also contain the experimental data provided in EXFOR (19), with points labelled in the key according to the originating author and year of publication. The figures highlight the discrepancies in the nuclear data libraries and the lack of experimental data for neutrons at energies around 14 MeV, i.e. the energy of neutrons born in the DT fusion reaction.

The cross-section data for O isotopes in TENDL-2021 was taken from JEFF-3.3 (11), but it is clear that the cross-section for  $^{17}\text{O}(\text{n},\alpha)^{14}\text{C}$  reaction in TENDL-2021 files does not match the cross-section given in the JEFF-3.3 (possibly due to an error in the processing of nuclear data files). In the past, similar discrepancies were noticed in the TENDL data libraries. In TENDL-2017 and TENDL-2019 (20; 21), the cross-section data for  $^{17}\text{O}$  was said to be taken from the ENDF/B-VIII.0 library, but only the TENDL-2019 cross-sections matched ENDF/B-VIII.0 evaluations. These discrepancies further add to the overall ambiguity in  $^{14}\text{C}$  production from O isotopes. In the case of  $^{18}\text{O}(\text{n},\text{n}'\alpha)^{14}\text{C}$  reaction channel (Fig. 4), only one experimental data point is available (22). In the case of  $^{17}\text{O}(\text{n},\alpha)^{14}\text{C}$  reaction (Fig. 3) channel, more data points are available at the keV range, but again, only one at the fusion energy relevant

range (23; 22). The data point at 14 MeV, in both reaction channels, was taken from the FNS experiment, but none of the nuclear data libraries, except JENDL-5.0, agree with that experimental data (24).

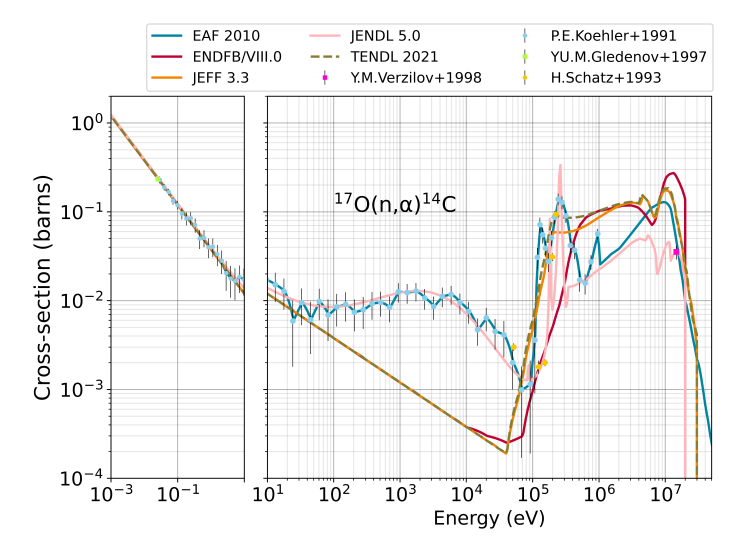


Figure 3:  $(n,\alpha)$  Reaction cross-section for <sup>14</sup>C production from <sup>17</sup>O, comparing the evaluations from several different nuclear data libraries with the available experimental data points in EXFOR.

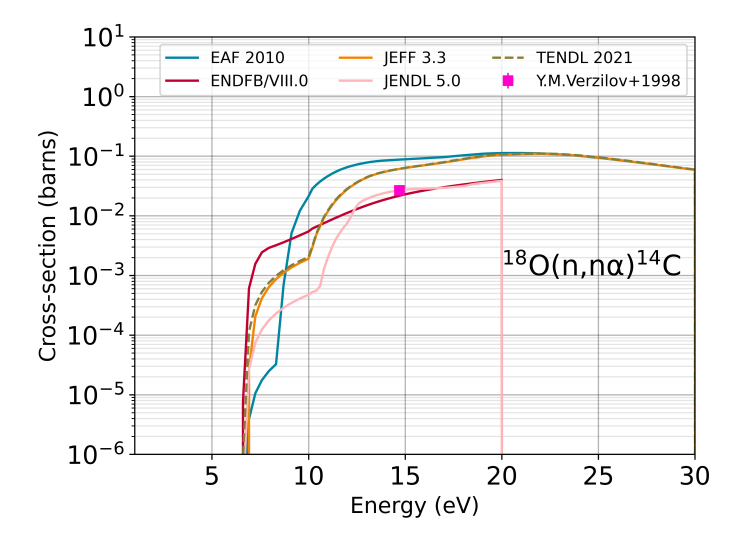


Figure 4:  $(n,n'\alpha)$  Reaction cross-section for <sup>14</sup>C production from <sup>18</sup>O, comparing the evaluations from several different nuclear data libraries with the available experimental data points in EXFOR.

These discrepancies in the cross-section would lead to uncertainty in the production of  $^{14}\mathrm{C}$  and thus its activity. Since the  $^{17}\mathrm{O}(\mathrm{n},\alpha)^{14}\mathrm{C}$  reaction cross-section is much higher at low energies, this reaction channel is relevant for both fission and fusion reactor conditions. But the  $^{18}\mathrm{O}(\mathrm{n},\mathrm{n}'\alpha)^{14}\mathrm{C}$  reaction channel has a threshold of 6.3 MeV and thus is only relevant for fusion energy applications.

To study the difference in <sup>14</sup>C production due to the differences in the cross-section evaluations at various energy ranges, neutron spectra from both fusion and fission systems are used.

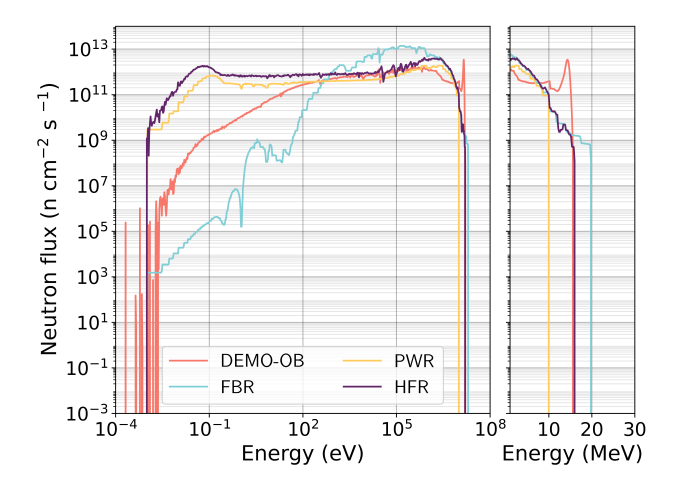


Figure 5: Various neutron spectra used in the study. Left: the spectra on a logarithmic eV scale showing the full energy range. Right: a linear MeV scale showing the high-energy parts of the spectra, in particular the fission tails.

The different neutron spectra used in the study are given in Fig. 5.

These spectra were taken from the FISPACT-II wiki (25), and a short summary of neutron spectra used in the calculations is given below:

- DEMO-OB is the Outboard Blanket spectrum obtained for the 2017 European DEMO baseline design with total integrated flux of 2.19 × (10<sup>14</sup> n cm<sup>-2</sup> s<sup>-1</sup>) (1; 2).
- FBR is the core assembly spectrum for the large-scale prototype fast breeder Superphenix reactor that was located in the south of France  $(1.2 \times 10^{15} \text{ n cm}^{-2} \text{ s}^{-1})$  (26).
- HFR is the spectrum for volume-averaged low-flux material test location of the high-flux reactor at Petten, Netherlands  $(5.3 \times 10^{14} \text{ n cm}^{-2} \text{ s}^{-1})$  (27).
- and PWR is the fuel assembly-averaged spectrum for the type P4 pressurized-water reactor at the Paluel site in France  $(3.25 \times 10^{14} \text{ n cm}^{-2} \text{ s}^{-1})$  (28).

#### 3. Calculation methodology

Analytical calculations are carried out for the above-mentioned production channel reactions,  $^{17}O(n,\alpha)^{14}C$  and  $^{18}O(n,n'\alpha)^{14}C$  for every nuclear data library with the different incident neutron spectra.

The change in concentration of any isotope as a function of time in a neutron environment is given by the differential equation:

$$\frac{dN_i}{dt} = -(\lambda_i + \sigma_i \phi) N_i + \sum_{i \neq i} (\lambda_{ij} + \sigma_{ij} \phi) N_j$$
 (1)

where  $N_i$  = number of nuclide i at time t

 $\lambda_i$  = total decay constant of nuclide i (s<sup>-1</sup>)

 $\sigma_i$  = total cross-section for reactions on i (cm<sup>2</sup>)

 $\lambda_{ij}$  = decay constant of nuclide j producing i (s<sup>-1</sup>)

 $\sigma_{ij}$  = reaction cross-section for reactions on j producing i (cm<sup>2</sup>)  $\phi$  = neutron flux (cm<sup>-2</sup>s<sup>-1</sup>)

As  $^{14}\text{C}$  has a very long half-life, it will not decay significantly within the operation times of any nuclear reactor (thus, we can consider  $\lambda_i$  to be zero). And since  $^{14}\text{C}$  has low concentration in the material and the production pathway from its parent nuclides dominates the equation, the neutron-induced burnup ( $\sigma_i \phi \approx 0$ ) of  $^{14}\text{C}$  can also be neglected. Also, we are exploring the impact of the single one-step reaction, and so the rate of production of  $^{14}\text{C}$  ( $\frac{dN_i}{dt}$ ) from a single reaction from a parent ( $N_j$ ) can be approximated (to first order) as:

$$\frac{dN_i}{dt} \approx \sigma \phi N_j \tag{2}$$

Integrating the above equation, the amount of <sup>14</sup>C at any time t for the group-wise neutron spectra can be estimated using:

$$N_i(t) = (1 - e^{-(\sum_g \sigma_g \phi_g)t}) N_i(0)$$
 (3)

where  $N_i(t)$  is the number of atoms of <sup>14</sup>C at time t,  $N_j(0)$  is initial number of atoms of parent nuclide (<sup>17</sup>O or <sup>18</sup>O),  $\sigma_g$  is the group-wise reaction cross-section for production of <sup>14</sup>C from parent j,  $\phi_g$  is the group-wise neutron spectrum incident on the parent nuclide j and t is the time of the irradiation.

In this study, <sup>17</sup>O and <sup>18</sup>O present in 1 kg of KALOS are irradiated with the neutron spectrum given in Fig. 5 for 5 FPY; 1 Full Power Year (FPY) is equivalent to the continuous operation of the reactor for one year with 100% availability. The irradiation period of 5 FPY was selected in this study because it is the planned lifetime for EU-DEMO (29). The specific activity of <sup>14</sup>C generated in 1 kg of KALOS through the individual reaction channels is then compared among the nuclear data libraries and against the waste classification limits.

The cross-section values used in this study for the nuclear data libraries like EAF-2010, JEFF-3.3 and ENDF/B-VIII.0 were generated using the FISPACT-II EXTRACTXS functionality (30; 31). Since the TENDL-2021 (only available in the 1102 group structure) and JENDL-5.0 evaluations were not available in the 709 group structure for FISPACT-II simulations, we processed the libraries in the desired group structure using NJOY-2021 (32).

#### 4. Results

The reaction rate per unit of lethargy and the activity of the  $^{14}\text{C}$  produced via  $^{17}\text{O}(\text{n},\alpha)^{14}\text{C}$  and  $^{18}\text{O}(\text{n},\text{n}'\alpha)^{14}\text{C}$  reaction are compared for the nuclear data libraries for different neutron spectra. The results are summarised in the sections below. The activity of  $^{14}\text{C}$  is also compared against the UK global limit on  $\beta\gamma$  activity for Low-Level Waste (LLW) classification and the French waste classification limits (33).

#### 4.1. $^{14}C$ production from $^{17}O(n,\alpha)^{14}C$ reaction

The reaction rate is the summation term,  $\sum_g \sigma_g \phi_g$ , in the Eq 3. The reaction rate per unit lethargy for  $^{17}\text{O}(\text{n},\alpha)^{14}\text{C}$  for different data libraries in various neutron environments is plotted in Fig. 6. Differences in the reaction rates, calculated for all the libraries, can be observed at all energy ranges and for all

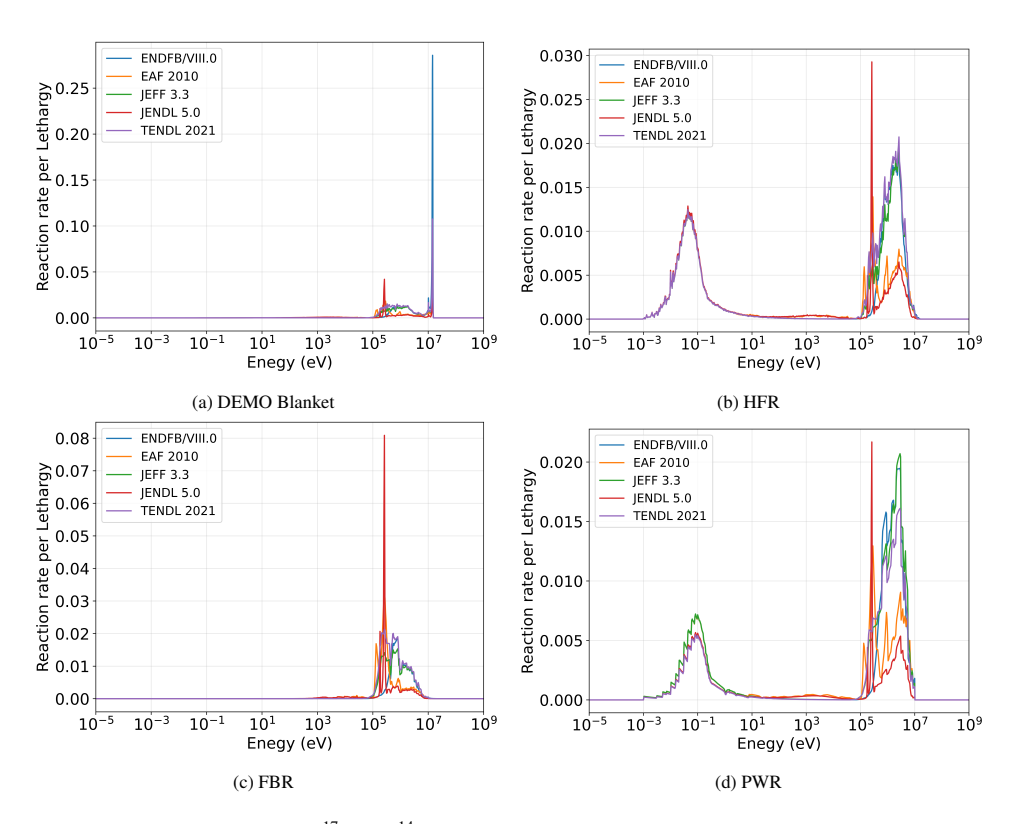


Figure 6: The reaction rate per unit lethargy for  $^{17}O(n,\alpha)^{14}C$  channel for various nuclear data libraries for different incident neutron spectra

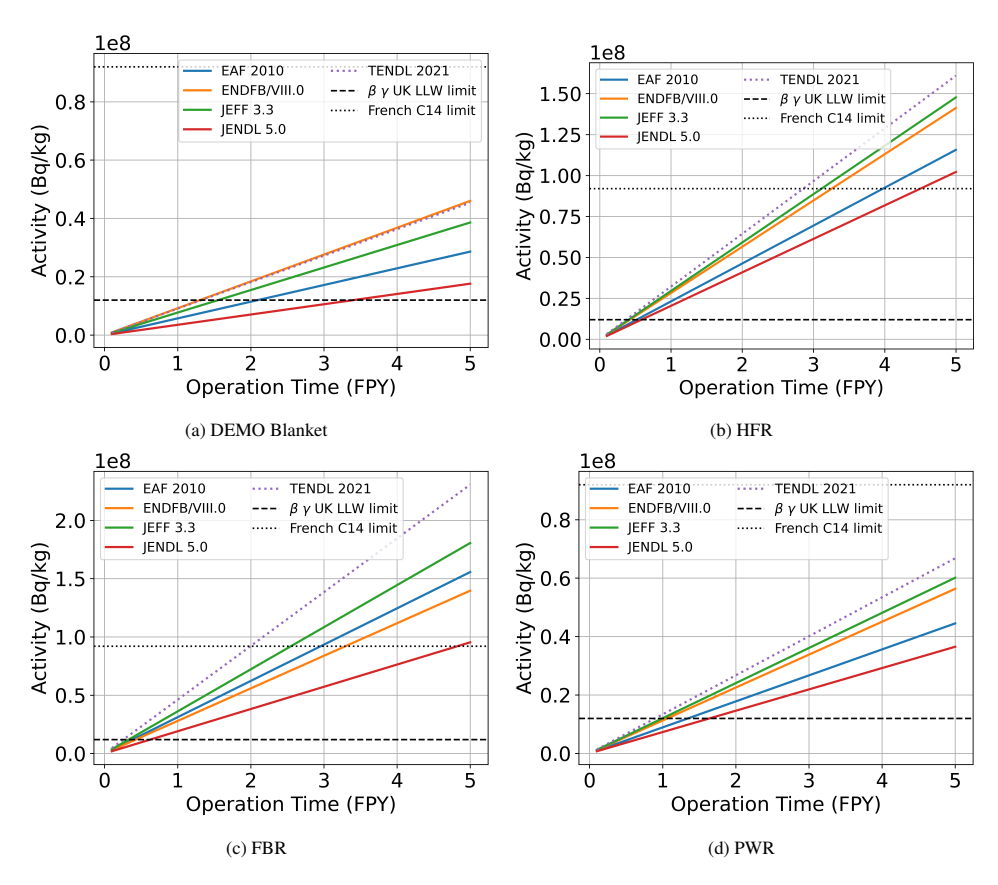


Figure 7:  $^{14}$ C activity from all the  $^{14}$ C created via the  $^{17}$ O(n, $\alpha$ ) $^{14}$ C reaction channel for different nuclear data libraries using the analytical calculation for different incident neutron spectra.

neutron spectra studied here. Among all libraries, the reaction rates are the highest for the DEMO blanket spectrum (Fig. 6a) due to the higher neutron flux in the fast region.

The <sup>14</sup>C production from <sup>17</sup>O using the analytical solution of Equation 3 for 5 FPY operation is given in Fig. 7. The UK and French disposal limits for <sup>14</sup>C are also plotted in the figures to highlight that the <sup>14</sup>C activity would exceed the regulatory limits at different times depending on the nuclear data library used. In the case of the DEMO blanket neutron spectra ( see Fig. 7a), TENDL-2021 and ENDF/B-VIII.0 predict the highest amount of the <sup>14</sup>C activity, and JENDL-5.0 predicts the lowest. After 5 FPY, the difference between the highest and lowest prediction is more than a factor of 2. The operation time taken by TENDL-2021 and ENDF/B-VIII.0 to breach the UK  $\beta\gamma$  LLW limit is less than 1.5 FPY, whereas for JENDL-5.0 it is close to 3.5 FPY. So, depending on the data library used, engineers performing waste assessment simulations would draw very different conclusions on the <sup>14</sup>C activity for waste classification, processing and disposal. Furthermore, choosing the best nuclear data library for such calculations becomes difficult since experimental data is scarce.

The High Flux Reactor (HFR) has significant neutron flux at all energies and has two peaks in the reaction rate (see Fig. 6b). At low energies, the reaction rate is similar for different libraries, but at high energies, there is a large discrepancy in the prediction from different data libraries. The <sup>14</sup>C activity when irradiated with HFR neutron spectrum using different nuclear data libraries is given in Fig. 7b. In this case, TENDL-2021 again predicts the highest activity for <sup>14</sup>C, but ENDF/B-VIII.0 predicts a lower value. After irradiation for 5 FPY, the difference between the highest and lowest prediction is almost 60%. In the HFR neutron environment, the <sup>14</sup>C activity crosses the French ILW limits within 3 FPY for TENDL-2021 and within 4.5 FPY for JENDL-5.0. This implies that although, according to all the data libraries, the material placed in HFR will be classified as ILW in the UK, there would be uncertainty about its classification according to French waste limits.

The reaction rate and the  $^{14}$ C activity in the Superphenix reactor (FBR) neutron environment are given in Fig. 6c and Fig. 7c respectively. Since there is a large discrepancy in the reaction rate among the different libraries, there is also a large discrepancy in the  $^{14}$ C production. Also, since FBR has the highest total integrated neutron flux,  $^{14}$ C activity is the highest among all the different neutron environments. Again, TENDL-2021 predicts the highest activity for  $^{14}$ C, crossing the French  $^{14}$ C limit after 2 FPY of operation. With JENDL-5.0, it takes close to 5 FPY to cross the same limit. All the libraries predict  $^{14}$ C activity higher than the UK global limit on  $\beta\gamma$  activity. The difference between the highest and lowest prediction is more than a factor of 2 at the end of 5 FPY.

The reaction rate calculated for the neutron spectrum in the Paluel light water reactor (PWR) also has two peaks, one at the low energies and the other at the high energies (see Fig. 6d). However, due to the lower total integrated neutron flux, the amount of <sup>14</sup>C is lower than other fission reactors but comparable to DEMO blanket (see Fig. 7d). Again, TENDL-2021 predicts the highest activity, and JENDL-5.0 predicts the low-

est. Unlike HFR and FBR, the  $^{14}$ C does not cross the French  $^{14}$ C limit within 5 FPY but does cross the UK  $\beta\gamma$  LLW limit within 2 FPY for all nuclear data libraries. The difference between the highest and lowest prediction is 80% at the end of 5 FPY irradiation.

#### 4.2. $^{14}C$ production from $^{18}O(n,n'\alpha)^{14}C$ reaction

The  ${}^{18}\text{O}(\text{n,n'}\alpha){}^{14}\text{C}$  reaction is a threshold reaction, so only the neutrons above 6.3 MeV would interact with <sup>18</sup>O atoms. This means that even though <sup>18</sup>O is more abundant than <sup>17</sup>O, the <sup>14</sup>C production predicted through this reaction is significantly lower. The reaction rate and the 14C activity for each library in different neutron environments is given in Figures 8, 9 respectively. Only in the DEMO Blanket neutron spectrum( see Fig. 9a), the activity of <sup>14</sup>C produced is significantly higher than the UK global LLW limit on  $\beta \gamma$  activity for some data libraries. This creates an issue for the waste classification as the waste characterisation depends on the nuclear data library used. For the fission neutron environments (see Fig. ??), the activity of <sup>14</sup>C produced is not significant. However, these results still highlight the issue of large discrepancies between the different libraries. Furthermore, since only one experimental data point is available at high energy region, the validity of all the values in nuclear data libraries for  $^{18}O(n,n'\alpha)^{14}C$  reaction can be questioned. The important point to note here is that in an O-rich material, the total activity of <sup>14</sup>C produced would be the sum of the <sup>14</sup>C produced from <sup>17</sup>O(n, $\alpha$ ) <sup>14</sup>C and <sup>18</sup>O(n,n' $\alpha$ ) <sup>14</sup>C reaction channels. Since  $^{14}$ C produced from  $^{17}$ O(n, $\alpha$ ) $^{14}$ C is higher than the waste classification limits in most cases, the <sup>14</sup>C produced from  $^{18}O(n,n'\alpha)^{14}C$  reaction would only add to it.

#### 5. Uncertainty analysis

Discrepancies are also present in the uncertainty data and covariance matrices given in the nuclear data libraries. JENDL-5.0, EAF-2010 and ENDF/B-VIII.0 data libraries contain no covariance matrices. A closer analysis of the covariance matrices of the TENDL libraries and JEFF3.3 shows severe inconsistencies and deficiencies which do not inspire confidence in the nuclear data predictions. For the  $^{17}O(n,\alpha)$  covariance matrices:

- In TENDL-2021, the correlations are provided for the whole energy range, but the standard deviations are (close to) zero below ~ 100 keV.
- JEFF-3.3 covariance data start at even higher neutron energies, covering only the energy range between ~ 0.3 to 20 MeV.
- Only TENDL-2017 spans down to thermal energies; however, the reported standard deviations seem unrealistically large/huge (up to a few 1000 %, indicating (a) possible scaling error(s)). Even though newer versions of TENDL libraries are available, TENDL-2017 is the only evaluation which has non-zero uncertainty for  $^{17}O(n,\alpha)^{14}C$  reaction channel at thermal energies, and hence is considered in this study.

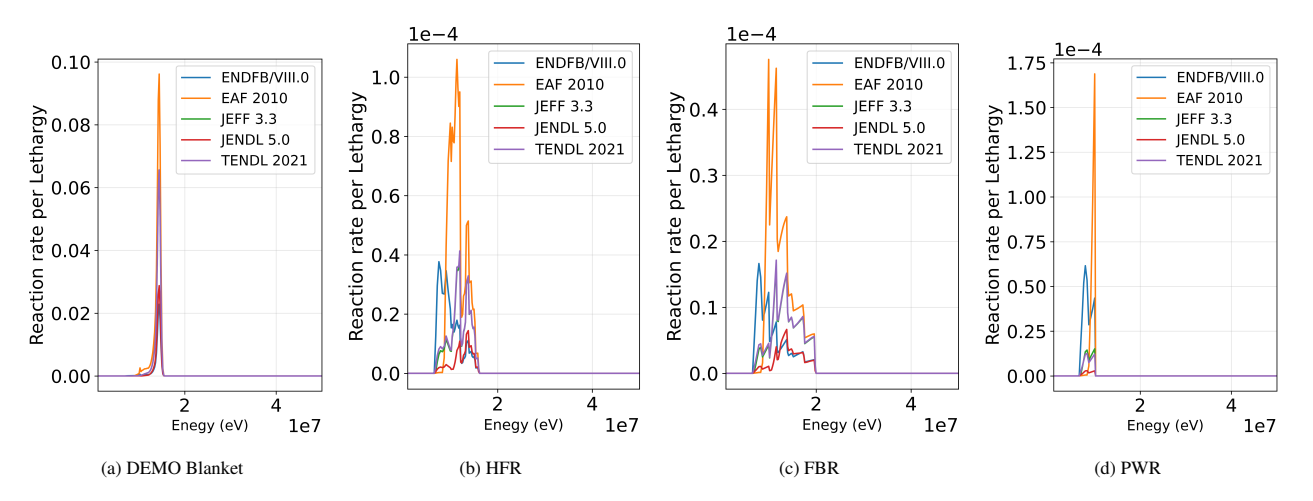


Figure 8: The reaction rate per unit lethargy for  $^{18}O(n,n'\alpha)^{14}C$  channel for various nuclear data libraries for different incident neutron spectra

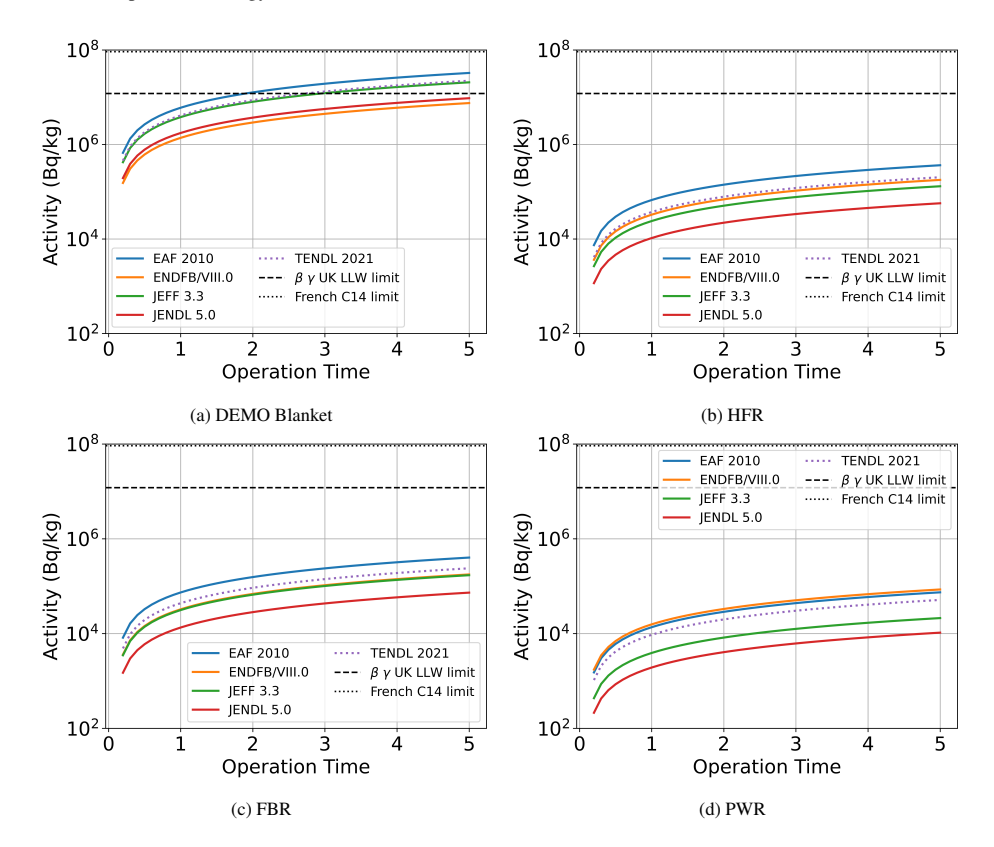


Figure 9:  $^{14}$ C activity from all the  $^{14}$ C created via the  $^{18}$ O(n,n' $\alpha$ ) $^{14}$ C reaction channel for different nuclear data libraries using the analytical calculation for different incident neutron spectra.

The uncertainty in  $^{14}$ C production in DEMO Blanket due to the uncertainties in the underlying  $(n,\alpha)$  cross sections was calculated using the SUSD3D code (10). SUSD3D, a multi-dimensional nuclear cross-section sensitivity and uncertainty code, uses first-order generalised perturbation theory to calculate the sensitivity coefficients and standard deviation in the calculated detector responses or design parameters of interest  $(k_{eff}, \beta_{eff})$ , reaction rates) due to input cross-section data and their covariance matrices. As demonstrated in Table 1 the differences in the available covariance matrices result in huge differences among the uncertainty predictions for  $^{14}$ C production,

with the uncertainty in  $^{17}O(n,\alpha)$  reaction rate ranging from 3 to over 3000 %, and the one in  $^{18}O(n,n'\alpha)$  reaction rate from 5 to 24 %. Furthermore, the uncertainties are in general not consistent with the differences in  $^{14}C$  production observed using different nuclear data libraries (see Figs. 6 and 7), nor with the differences between the measured and the evaluated cross sections (see Fig. 3).

	Uncertainty (%)					
Covariance →	<sup>17</sup> O			<sup>18</sup> O		
Cross-sections	JEFF3.3	TENDL2017	TENDL2021	JEFF3.3	TENDL2021	
JEFF3.3	19.2	115.5	5.8	23.9	5.4	
ENDF/B-VIII.0	21.3	97.3	7.4	23.1	5.2	
JENDL5.0	15.0	668.5	5.2	24.2	5.4	
TENDL2017	8.5	3503.5	2.8	24.0	5.4	
TENDL2021	19.2	115.5	5.8	23.9	5.4	

Table 1: Uncertainty in the  $^{17}O(n,\alpha)$  and  $^{18}O(n,n'\alpha)$  reaction rates in DEMO Blanket calculated using the cross sections and covariance matrices taken from JEFF3.3, TENDL-2017 and -2021 (calculated using the SUSD3D code (10)).

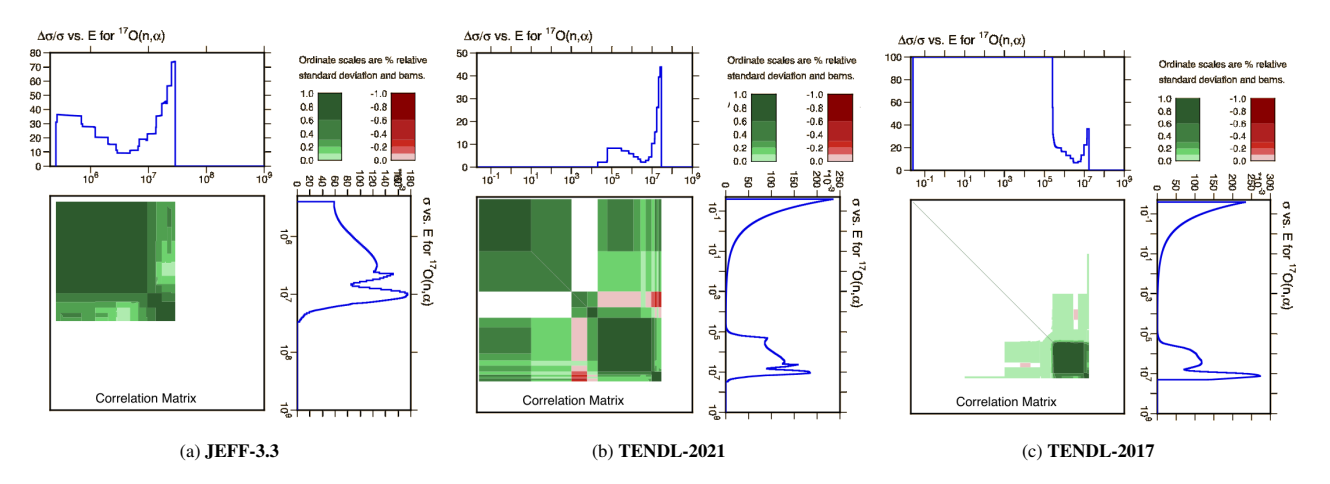


Figure 10: Covariance matrices of  $^{17}O(n,\alpha)$  reaction channel from the JEFF-3.3, TENDL-2021 and TENDL-2017 evaluations.

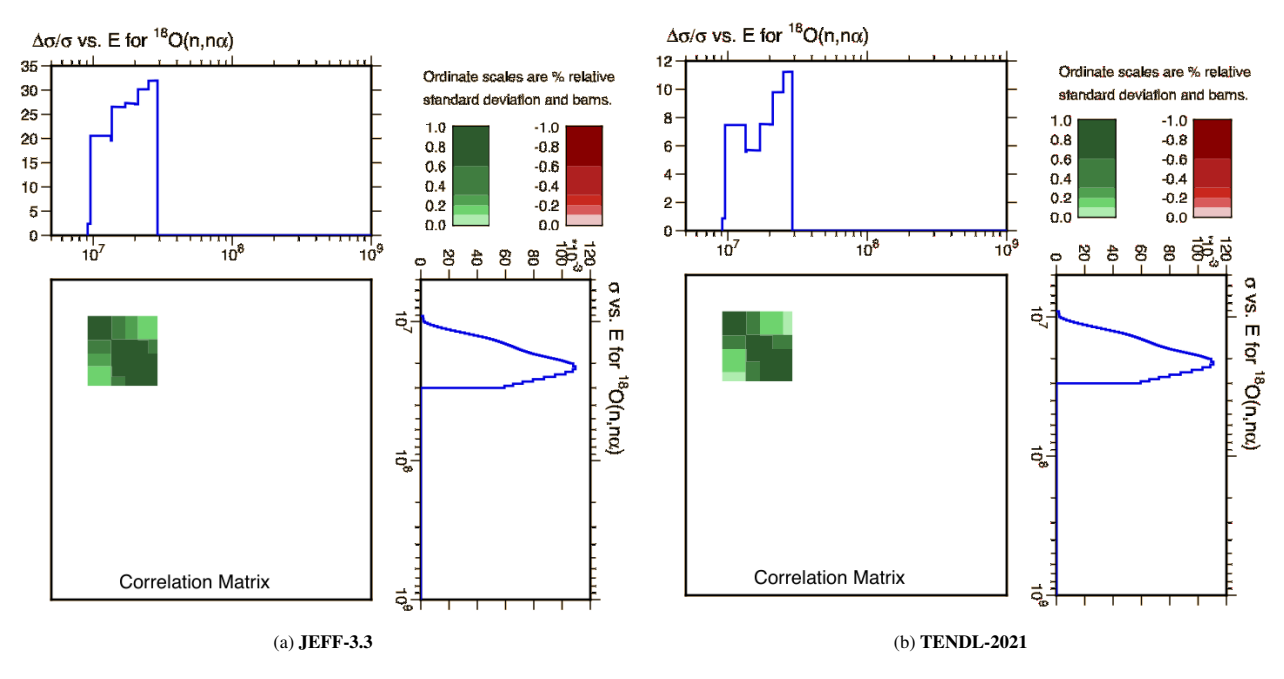


Figure 11: Covariance matrices of  $^{18}O(n,n'\alpha)$  from the JEFF-3.3 and TENDL-2021 evaluations.

### 6. Additional findings - Discrepancies in reaction probabilities

The probability of a daughter being produced when the parent nuclide undergoes a nuclear reaction can be calculated using the PATHFINDER (3). The probabilities calculated using

the ENDF/B-VIII.0 nuclear data library are given in Fig. 1, and the probabilities calculated using the JEFF-3.3 nuclear data library are given in Fig. 12. The difference in the probability for  $^{14}$ C production from  $^{17}$ O(n, $\alpha$ ) $^{14}$ C reaction is due to the difference in  $^{17}$ O(n,2n') $^{16}$ O reaction cross-section in the two data

libraries. The  $^{17}O(n,2n')^{16}O$  reaction has different threshold energies, 4.36 MeV in the case of JEFF-3.3 and 7.58 MeV in the case ENDF/B-VIII.0. This would lead to a difference in the reaction rate and thus in the probability of creation of the daughter nuclide. In the case of  $^{18}O(n,n'\alpha)^{14}C$  reaction, the difference in

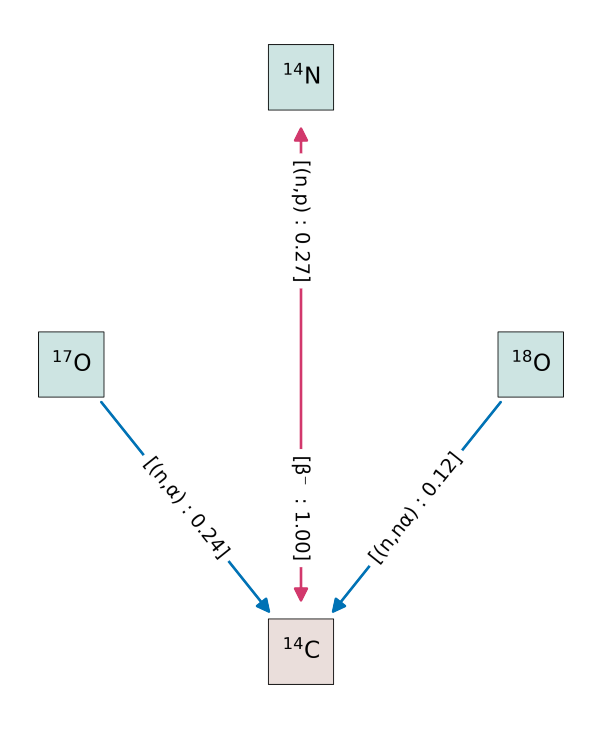


Figure 12: Pathways for production of <sup>14</sup>C using JEFF 3.3 data library

the production probability is due to the difference in the cross-section values of  $^{18}O(n,\alpha)^{15}C$  and  $^{18}O(n,2n')^{17}O$  reaction in the ENDF/B-VIII.0 and the JEFF-3.3 nuclear data libraries.

#### 7. Summary and conclusions

Assessment of <sup>14</sup>C in radioactive materials is crucial for assessing the hazards arising from waste recycling and disposal. Among three important channels for producing <sup>14</sup>C, we observed that the production pathways from O isotopes are not very well studied. Large differences and inconsistencies were observed in different nuclear data libraries, both in cross-section and covariance matrices, and both need further work supported by experimental validation. These large discrepancies in the nuclear data libraries present issues for calculating the production of <sup>14</sup>C using inventory codes like FISPACT-II. Since the FISPACT-II outputs are used to predict waste severity, the discrepancy in <sup>14</sup>C inventory could lead to a discrepancy in resulting waste classification. Furthermore, the available nuclear data covariance information leads to unrealistic estimation of uncertainties in <sup>14</sup>C production.

The lack of experimental data at high energies adds to the ambiguity of <sup>14</sup>C production. The previous experiment to evaluate the <sup>14</sup>C production from O isotopes was done more than 20 years ago. With the EU-DEMO focusing on the HCPB blanket

concept containing large amounts of oxygen, conducting additional high-precision experiments at fusion-relevant energies becomes crucial.

#### Acknowledgements

This work has been funded by the EPSRC Energy Programme [grant number EP/W006839/1]. To obtain further information on the data and models underlying this paper please contact PublicationsManager@ukaea.uk

#### References

- T.A. Berry, T. Eade, C. Bachmann, A. Čufar, T. Franke, C. Gliss, D. Leichtle, and C. Vorpahl. Shutdown dose rates in-cryostat outside the EU-DEMO vacuum vessel. <u>Fusion Engineering and Design</u>, 193:113619, 2023
- [2] G.W. Bailey, M.R. Gilbert, T.A. Berry, T. Eade, C. Bachmann, and U. Fischer. Current status of DEMO activated waste studies. In <u>Proceedings of</u> 28th IAEA Fusion Energy Conference (FEC 2020), 2021.
- [3] P. Kanth, M.R. Gilbert, and D. Foster. PATHFINDER: A tool for calculating pathways for fusion-activated materials. In <u>31st International</u> Conference Nuclear Energy for New Europe, 2022.
- [4] R. Knitter, M.H.H. Kolb, U. Kaufmann, and A.A. Goraieb. Fabrication of modified lithium orthosilicate pebbles by addition of titania. <u>Journal of Nuclear Materials</u>, 442(1, Supplement 1):S433–S436, 2013. FIF-TEENTH INTERNATIONAL CONFERENCE ON FUSION REACTOR MATERIALS.
- [5] M.H.H. Kolb, K. Mukai, R. Knitter, and T. Hoshino. Li<sub>4</sub>SiO<sub>4</sub> based breeder ceramics with Li<sub>2</sub>TiO<sub>3</sub>, LiAlO<sub>2</sub> and Li<sub>X</sub>La<sub>Y</sub>TiO<sub>3</sub> additions, part I: Fabrication. Fusion Engineering and Design, 115:39–48, 2017.
- [6] Management of Waste Containing Tritium and Carbon-14. Number 421 in Technical Reports Series. INTERNATIONAL ATOMIC ENERGY AGENCY, Vienna, 2004.
- [7] Sehila M. Gonzalez de Vicente, Nicholas A. Smith, Laila El-Guebaly, Sergio Ciattaglia, Luigi Di Pace, Mark Gilbert, Robert Mandoki, Sandrine Rosanvallon, Youji Someya, Kenji Tobita, and David Torcy. Overview on the management of radioactive waste from fusion facilities: ITER, demonstration machines and power plants. <u>Nuclear Fusion</u>, 62(8):085001, may 2022.
- [8] M.R. Gilbert, T. Eade, T. Rey, R. Vale, C. Bachmann, U. Fischer, and N.P. Taylor. Waste implications from minor impurities in European DEMO materials. Nuclear Fusion, 59(7):076015, may 2019.
- [9] Oliver Leys, Julia M. Leys, and Regina Knitter. Current status and future perspectives of eu ceramic breeder development. <u>Fusion Engineering and</u> Design, 164:112171, 2021.
- [10] I. Kodeli. XSUN-2022/SUSD3D n/γ sensitivity-uncertainty code package with recent JEFF-3.3 and ENDF/B-VIII.0 covariance data. EPJ Web Conf., 281:7, 2023.
- [11] A. J. Koning, D. Rochman, and J.-Ch. Sublet. TENDL 2021: Talys-based evaluated nuclear data library, 2021.
- [12] A.J. Koning, D. Rochman, J.-Ch. Sublet, N. Dzysiuk, M. Fleming, and S. van der Marck. TENDL: Complete nuclear data library for innovative nuclear science and technology. <u>Nuclear Data Sheets</u>, 155:1–55, 2019. Special Issue on Nuclear Reaction <u>Data</u>.
- [13] The JEFF team. JEFF-3.3: evaluated nuclear data library, 2017.
- [14] A. J. M. Plompen et al. The joint evaluated fission and fusion nuclear data library, JEFF-3.3. <u>Eur. Phys. J. A</u>, 56(7):181, 2020.
- [15] J.-Ch. Sublet et al. The european activation file: Eaf-2010 neutroninduced cross section library. Technical report, United Kingdom Atomic Energy Authority, 2010.
- [16] O. Iwamoto, N., S. Kunieda, F. Minato, S. Nakayama, Y. Abe, K. Tsubakihara, S. Okumura, C. Ishizuka, T. Yoshida, S. Chiba, N. Otuka, J.-Ch. Sublet, H. Iwamoto, K. Yamamoto, Y. Nagaya, K. Tada, C. Konno, N. Matsuda, K. Yokoyama, H. Taninaka, A. Oizumi, M. Fukushima, S. Okita, G. Chiba, S. Sato, M. Ohta, and S. Kwon. Japanese evaluated nuclear data library version 5: JENDL-5. Journal of Nuclear Science and Technology, 60(1):1–60, 2023.

- [17] D. Brown et al. ENDF/B-VIII.0 nuclear data for science and technology, 2018
- [18] D.A. Brown et al. ENDF/B-VIII.0: The 8th major release of the nuclear reaction data library with CIELO-project cross sections, new standards and thermal scattering data. <u>Nuclear Data Sheets</u>, 148:1–142, 2018. Special Issue on Nuclear Reaction Data.
- [19] N. Otuka et al. Towards a more complete and accurate experimental nuclear reaction data library (exfor): International collaboration between nuclear reaction data centres (nrdc). <u>Nuclear Data Sheets</u>, 120:272–276, 2014
- [20] A. J. Koning, D. Rochman, and J.-Ch. Sublet. TENDL 2017: Talys-based evaluated nuclear data library, 2017.
- [21] A. J. Koning, D. Rochman, and J.-Ch. Sublet. TENDL 2019: Talys-based evaluated nuclear data library, 2019.
- [22] Y. M. Verzilov, Y. Ikeda, F. Maekawa, Y. Oyama, and D. L. Smith. Measurements of tritium and 14c production cross sections for 14.7-mev neutrons on 17o and 18o. <u>Nuclear Science and Engineering</u>, 129(1):81–87, 1008
- [23] H. Schatz, F. Kaeppeler, P. E. Koehler, M. Wiescher, and H. P. Trautvetter. 17O(n, alpha) 14C: Closure of a Primordial CNO Bi-Cycle? Astrophysical Journal, 413:750, August 1993.
- [24] F. Maekawa, K. Shibata, M. Wada, Y. Ikeda, and H. Takeuchi. Comprehensive activation experiment with 14-mev neutrons covering most of naturally existing elements 5 minutes irradiation experiment —. <u>Journal</u> of Nuclear Science and Technology, 39(sup2):990–993, 2002.
- [25] FISPACT-II wiki main page. Accessed: 2023-09-26.
- [26] FISPACT-II wiki Fast breeder reactor, Superphénix. Accessed: 2023-09-26.
- [27] FISPACT-II wiki Material test reactor, Petten HFR high. Accessed: 2023-09-26.
- [28] FISPACT-II wiki Paluel light water reactor. Accessed: 2023-09-26.
- [29] G. Caruso, S. Ciattaglia, B. Colling, L. Di Pace, D.N. Dongiovanni, M. D'Onorio, M. Garcia, X.Z. Jin, J. Johnston, D. Leichtle, T. Pinna, M.T. Porfiri, W. Raskob, N. Taylor, N. Terranova, and R. Vale. DEMO the main achievements of the pre concept phase of the safety and environmental work package and the development of the gssr. <u>Fusion Engineering and Design</u>, 176:113025, 2022.
- [30] G.W. Bailey, D. Foster, P. Kanth, and M.R. Gilbert. <u>The FISPACT-II User</u> Manual. UKAEA.
- [31] J.-Ch. Sublet, J.W. Eastwood, J.G. Morgan, M.R. Gilbert, M. Fleming, and W. Arter. FISPACT-II: An advanced simulation system for activation, transmutation and material modelling. <u>Nuclear Data Sheets</u>, 139:77–137, 2017. Special Issue on Nuclear Reaction Data.
- [32] J. L. Conlin, A.C. Kahler, A. P. McCartney, and D. A. Rehn. NJOY21: Next generation nuclear data processing capabilities. <u>EPJ Web Conf.</u>, 146:09040, 2017.
- [33] G.W. Bailey, O.V. Vilkhivskaya, and M.R. Gilbert. Waste expectations of fusion steels under current waste repository criteria. <u>Nuclear Fusion</u>, 61(3):036010, jan 2021.